Effect of indium incorporation, stimulated by UHV treatment, on the chemical, optical and electronic properties of ZnO thin film

Bedrouni, Mahmoud; Kharroubi, Bachir; Ouerdane, Abdellah; Bouslama, M'hammed; Guezzoul, M'hamed; Caudano, Yves; Bensassi, Kada Belmokhtar; Bousmaha, Mohamed; Bezzerrouk, Mohamed Amine; Mokadem, Azzeddine; Abdelkrim, Mahfoud

Published in:
Optical Materials

DOI:
10.1016/j.optmat.2020.110560

Publication date:
2021

Document Version
Peer reviewed version

Effect of indium incorporation, stimulated by UHV treatment, on the chemical, optical and electronic properties of ZnO thin film.

Mahmoud Bedrouni[1], Bachir Kharroubi[2], Abdellah Ouerdane[1,3], M'hammed Bouslama[1], M'hamed Guezzoul[1], Yves Caudano[4], Kada Belmokhtar Bensassi[5], Mohammed Bousmaha[2], Mohamed Amine Bezzerrouk[2], Azzeddine Mokadem[1,6] and Mahfoud Abdelkrim[1].*

1. *Laboratory of materials (LABMAT), National Polytechnique School (ENP) of Oran, BP 1523 Oran Mnaouar, Oran, Algeria.*
2. *Research Laboratory of Industrial Technologies, Faculty of Applied Sciences, University of Tiaret, Tiaret, Algeria.*
3. *University of Djilali Bounaama-Khemis Miliana, Ain Defla, Algeria.*
4. *University of Namur Institute of Structured Matter (NISM) Belgium.*
5. *Technology Laboratory of Electron Microscopy and Materials Science, University of Science and Mohamed Boudiaf of Oran, Algeria.*
6. *University of Hassiba Ben Bouali Chlef, Algeria.*

**** Corresponding author:*** *guezzoulmhamed@gmail.com*

Abstract

We show the importance of powerful and complementary analysis techniques XPS (X-rays Photoelectron Spectroscopy), AES (Auger Electron Spectroscopy), and UPS (UV Photoelectron Spectroscopy) associated with PL (Photoluminescence) to investigate the chemical composition, optical emission, and electronic structure of undoped ZnO (UZO) and In-doped ZnO (IZO) thin films at the contaminated and clean states. The growth process of films on the Si substrate is achieved by ultrasonic spray pyrolysis. Both samples are submitted in the same conditions to cleaning treatment (argon ion etching followed by thermal annealing in Ultra High Vacuum UHV). The XPS and AES results display the great interest of physical UHV treatment to eliminate the contamination layer and stimulate the incorporation and oxidation of indium into the ZnO matrix. The PL measurements confirm that the UHV treatment allows the incorporation of indium into the ZnO matrix and eliminates wholly the visible emission due to hydroxyl impurities and defects such as oxygen interstitial and oxygen vacancies. The UPS technique is useful to show the electronic structure of the valence band and determine the work function, Fermi level, and the ionization potential of both samples.

Keywords: *IZO thin film, UHV treatment, XPS, PL, structural defects and electronic structure.*

1. Introduction:

Zinc oxide (ZnO) has attracted the attention of researchers because of its great properties applied in the sciences and industry **[1]**. The wide and direct band gap of 3.37eV at room temperature **[2]**, the large exciton binding energy (60meV), the high carrier mobility and other useful properties **[3]** make ZnO suitable for a wide range of devices such as solar cell, supercapacitors, piezoelectric, UV photodetectors, photodiodes, flexible and porous 3-D ceramics, functional surface coating and sensors **[4]**. These applications with high quality and reliable performance are related to preparation mode and post-treatment process of the sample in order to improve the chemical, electrical, optical, and morphological properties.

ZnO is of low cost, no toxic and of high electron conductivity. It can replace the indium tin oxide (ITO) for the light-emitting contact layer and photovoltaics **[1]**. However, efforts are continuously being made to achieve high carrier concentration and mobility as well as transmittance to improve the performance of ZnO-based optoelectronic devices **[5-8].** As reported, the n-type conductivity in ZnO films occurs from intrinsic defects such as oxygen vacancies (V_O) and zinc interstitials (Zn_i). Dutta et al. **[9]** gave some results about the role of defects on the electrical properties of ZnO. Furthermore, doping ZnO films with Group III elements (Al, Ga, In, and B) advantaged to enhance its conductivity **[10-12].** The In-doping increased the carrier concentration of ZnO **[13-16]**. In-doped ZnO (IZO) film is of good electrical conductivity and transparency in the visible and IR ranges **[17-20]**, well appropriate to be applied as transparent electrodes, flat panel displays, solar cells and light-emitting diodes (LEDs) **[21-23]**.

Several studies have investigated the effect of doping by indium at low (1-5at%) **[24-31]**, moderate (5-10at%) **[26,29,32,33]** and high (>10at%) **[34,35]** concentrations on the structural, morphological, optical, and electrical properties of ZnO surfaces. Hsu et al. **[36]** reported that the oxygen vacancies concentration in the IZO thin films is reduced by increasing the indium doping concentration. Yu et al. **[37]** showed that the increase of In doping (0-7at%) improved the diode electroluminescence (LEDs) of n-ZnOp-GaN heterojunction. Hafdalla et al. **[29]** showed that the conductivity of In doped ZnO increases until to reach its maximum value with a concentration of indium of 6%. Chen et al. **[33]** suggested that the indium doping (5-9at%) reduces the structural defects and enhances the electrical conductivity. Based on these results, we suggest that it is very appropriate to study the effect of indium incorporation at moderate concentration (6at%) on the ZnO properties.

For this study, we have deposited the undoped and In (6%) doped ZnO in the same conditions using the ultrasonic spray pyrolysis. That technique is efficient in the preparation of thin film as pure and In doped ZnO **[6,38]**. There are many advantages of spray pyrolysis technique including its simplicity, cost-effectivity, non-vacuum required, variety of substrates, high deposition rate, and ability to deposit on broad areas **[39,40]**. However, the surface of ZnO thin film is susceptible to involve defects such as dangling bonds and / or hydroxyl groups as $Zn(OH)_2$ that limit the optical and electrical properties **[41].** Therefore, a post-treatment process is required for cleaning and improving the physical structure of the surface for better optical and electrical properties of applied ZnO films. However, the UZO and IZO thin films are treated in UHV conditions using argon ion etching followed by thermal annealing at high temperature (650°C). The effect of UHV treatment on the chemical, morphological and optical properties of undoped and Cu doped ZnO (UZO and CZO) was efficient for the surface treatment **[42]**. In this study, we use this physical treatment to stimulate the indium incorporation into the clean ZnO matrix with the aim to improve the optical and electronic properties of IZO compound. The investigation is done by using the sensitive and complementary techniques AES (Auger Electron Spectroscopy), XPS (X-Ray Photoelectron Spectroscopy) and UPS (UV Photoelectron Spectroscopy) associated with PL (Photoluminescence) measurements. These analysis techniques are of great sensitivity for checking the chemical composition, the physical and electronic structure, and the electron states in the gap of materials.

2. Experimental section:

2.1. Synthesis of undoped and In-doped ZnO thin films:

The UZO and IZO thin films were grown on Si substrate using the ultrasonic spray pyrolysis technique. The precursor solution of 0.4M (molar concentration) of UZO was prepared by dissolving zinc acetate dehydrate ($ZnC_4H_6O_4.2H_2O$) (Sigma Aldrich, 99%purity) into 100ml of methanol. For IZO, the indium chloride tetrahydrate ($InCl_3.4H_2O$) (Sigma Aldrich 98%) was used as dopant; the molar ratio concentration $[In]/([In]+[Zn])$ in the precursor solution was maintained at 6%. For both samples, the final solutions were stirred for 1 hour to obtain a homogeneous solution and sprayed using air as a carrier gas, over the preheated Si substrates at 400°C.

2.2.The process of UHV physical treatment:

The UZO and IZO thin films with the size of 1cm x 1cm were treated in the UHV system under the same experimental conditions using Ar ion etching followed by successive thermal annealing at 650°C. For the etching process, we use the ISE 5 scientaomicron ion source which operates over an energy range from 300 eV to 5 keV and can deliver a beam current of over 80 µA at 5 KeV. Low energy capability makes the ISE 5 ideal for cleaning sensitive samples and its focus element enables the ion beam to be focused onto the whole sample surface. We adjusted through a leak valve the pressure of argon at 2.10^{-6} mbar. The argon ions were accelerated by an energy of 1.2 KeV. The focus was set to deliver a 1 cm ion beam spot and generate a low ionic current of 3µA measured from the sample surface. The samples were submitted to the ion beam for 15 minutes. The thermal annealing process was gradually carried out using a standard manipulator with PBN (Pyrolytic Boron Nitride) resistive heater as follows: 350°C for 20 min, 500°C for 20 min and 650°C for 40 min.

2.3.Experimental equipment:

The room temperature photoluminescence (PL) was performed using He–Cd laser as an excitation source operating at 325 nm (3.81eV). This excitation energy is well appropriate to display the defect near band edge. The PL spectra were recorded using HORIBA spectrometer iHR-550 equipped with CCD detector (400-1000nm).

As shown in **table 1**, we give the experimental parameters for the recorded XPS, UPS and AES spectra. We use the scientaomicron systems “Omicron’s DAR 400 dual Mg/Al X-ray source”, “HIS 13 (High Intensity VUV source)” and “SL 1000 SPA electron beam source with filament type of LaB6” for XPS, UPS and AES analysis respectively. The anode voltage and emission current of X-ray source were set at 15KV and 15mA respectively allowing a source power of 225W. The spectra were recorded using the hemispherical Argus spectrometer of 128 channels with high resolution operating in Constant Analyzer Energy mode (CAE) for XPS and UPS and Constant Retard Ratio mode (CRR) for AES. The spectrometer was calibrated by using the photoelectron emission state Ag 3d5/2 at 368.2eV. The binding energies of XPS spectra were corrected on the basis of carbon (C 1s) at 284.8 eV. The chemical composition of UZO and IZO surfaces was investigated by calculating atomic concentrations (at%) of Zn, O, C and In using CasaXPS software, taking into account the relative sensitivity factors (RSF) of respective elements. UPS measurements are carried out with “HIS 13” helium gas discharge ($h\nu$=21.2 eV). The sample is connected to a negative

potential -6V. This sample bias is sufficient to separate sample analyzer cut-offs. Work function values and valence band maxima (VBM) are determined using linear extrapolation of the secondary electron cut-off feature and the leading edge of the valence band emissions, respectively.

<table>
<tr><th rowspan="2">Experimental analysis</th><th colspan="3">Sources</th><th colspan="3">Spectrometer: Argus of 128 channels</th></tr>
<tr><th>Type</th><th>Energy (eV)</th><th>Spot</th><th>Pass energy CAE/CRR</th><th>Dwell time (s)</th><th>Energy step (eV)</th></tr>
<tr><td>AES</td><td>SL 1000 SPA-LaB_6 (15-3500 eV)</td><td>3000</td><td>100-250µm</td><td colspan="2">CRR (%): 10</td><td rowspan="2">0.2</td><td rowspan="2">0.2</td></tr>
<tr><td>XPS</td><td rowspan="2">Omicron- DAR 400 dual Mg/Al X-ray</td><td>Al: 1486.7</td><td rowspan="2">0.5µm</td><td rowspan="3">CAE (eV)</td><td rowspan="2">50</td></tr>
<tr><td>X-AES</td><td>Mg:1253.6</td><td></td><td></td></tr>
<tr><td>UPS</td><td>HIS 13 (High Intensity VUV source)</td><td>He I: 21.2</td><td>1.7mm</td><td>2</td><td>0.4</td><td>0.02</td></tr>
</table>

Table 1: Experimental parameters of recorded AES, XPS and X-AES spectra. AES (Auger electrons induced by the electron excitation); XPS (Photoelectrons induced by the X Ray excitation), X-AES (Auger electrons induced by the X Ray excitation) and UPS (UV Photoelectron Spectroscopy)

3. Results and discussions

3.1.XPS and AES results of untreated surfaces (at the initial state):

The characterization of as-prepared UZO and IZO thin films (at the initial state) by XPS and AES techniques is necessary to investigate their chemical composition. The XPS survey spectra of UZO and IZO surfaces are shown in **figure 1-A.** The core-level peaks of Zn 2s, Zn 2p, In 3p, O 1s, In 3d, C 1s, Zn 3s, Zn 3p, Zn 3d and Auger transition peaks Zn LMM, In MNN, and O KLL are well identified. The atomic concentrations (at%) of Zn, In, O and C elements are calculated and given in the table on **figure 1-A**. The carbon is present on the surfaces as contamination layer confirmed by its high at% (47.98% for UZO and 52.02% for IZO). This leads to a significant decrease in the at% of Zn and In (12.02 and 1.64 % respectively), however, these ratios will show a great improvement after the UHV treatment in section 3.2. The well resolved Zn 2p3/2, O 1s, In 3d and C 1s spectra are shown in **figures 1-B**, **1-C**, **1-D** and **1-E** respectively. The binding energies of Zn 2p3/2 and O 1s of UZO thin film at 1021.75 eV and 530.5 eV respectively correspond to Zn-O bonds **[43]**. For IZO, the Zn 2p3/2 and O 1s peaks shifted slightly toward higher binding energies (Zn 2p3/2: ΔE=0.3eV, O

1s: ΔE=0.2eV). As reported by other authors **[13,14,45]**, these shifts can be ascribed to the difference in the electronegativity (χ) of Zn (χ = 1.65) and In (χ = 1.78). Because of that electronegativity difference, there is a valence electron density of zinc in Zn–O–In bond in IZO lower than the Zn–O–Zn one in UZO **[44]**. Consequently, there is a screening effect of Zn in IZO allowing to increase the binding energy of Zn 2p3/2 **[14,44]**. Furthermore, the incorporation of indium in the ZnO matrix is confirmed through the two characteristic peaks In 3d3/2 and In 3d5/2 at 444.8 eV and 452.3 eV respectively related to oxidized indium **[15]**. The XPS analysis does appear very sensitive to characterize the growth process performance of UZO and IZO achieved by the ultrasonic spray technique.

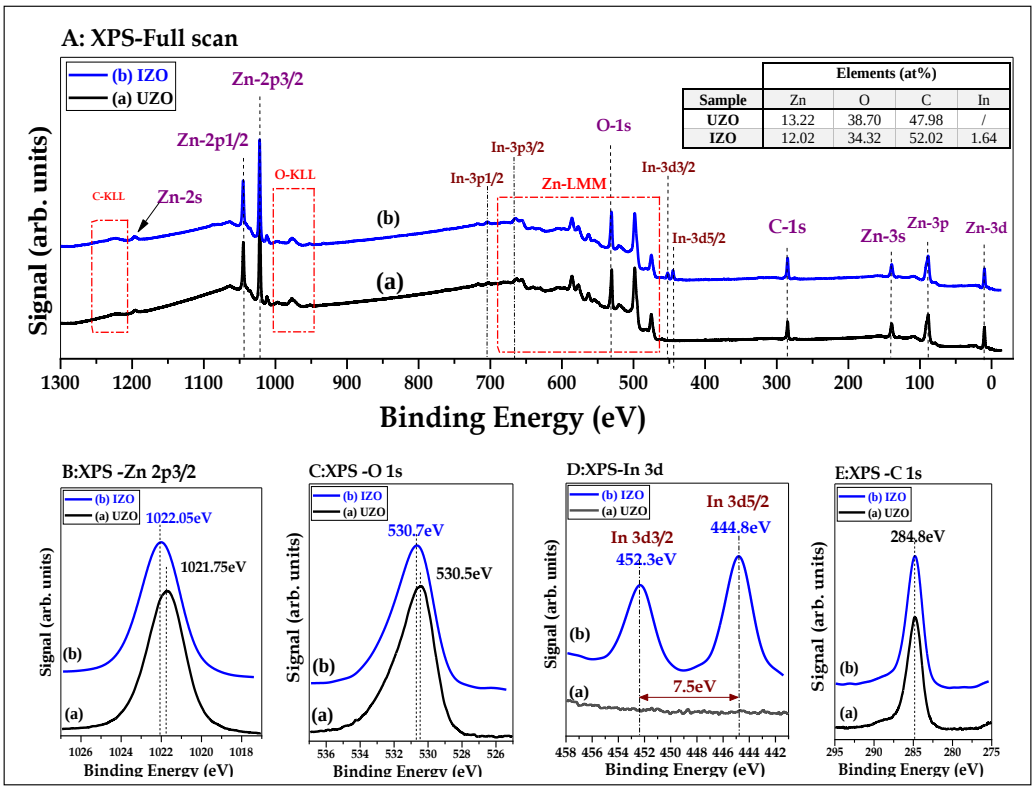

Figure 1: XPS spectra of as-prepared UZO(a) and IZO(b) thin films (at the initial state). A: full scan; B, C, D and E: the well-resolved photoemission spectra of Zn2p3/2; O-1s, In 3d and C 1s respectively.

The AES analysis is of high spatial resolution and very sensitive to chemical environment. The AES constitutes a good technique complementary to the XPS analysis. In this regard, **Figure 2** shows the AES and XAES spectra of UZO and IZO thin films at the initial state (as prepared). The Zn LMM and O KLL Auger signals are more intense in XAES spectra but less resolved than the AES ones (spectra D and E displaying shifts of 0.7eV and 1.4eV respectively). So, the Zn LMM and O KLL peaks of IZO shift towards lower kinetic energy

corresponding to electron states of higher binding energy in good concordance with the previous XPS results. The In MNN spectrum is of weak intensity and of broad shape. We will give a detailed discussion about this spectrum in section 3.2. The Auger signal C KLL is more resolved in figure 2 (I: AES, B: CKLL) because the AES analysis is of better sensitivity than XPS for the chemical elements of low atomic number (Z<30).

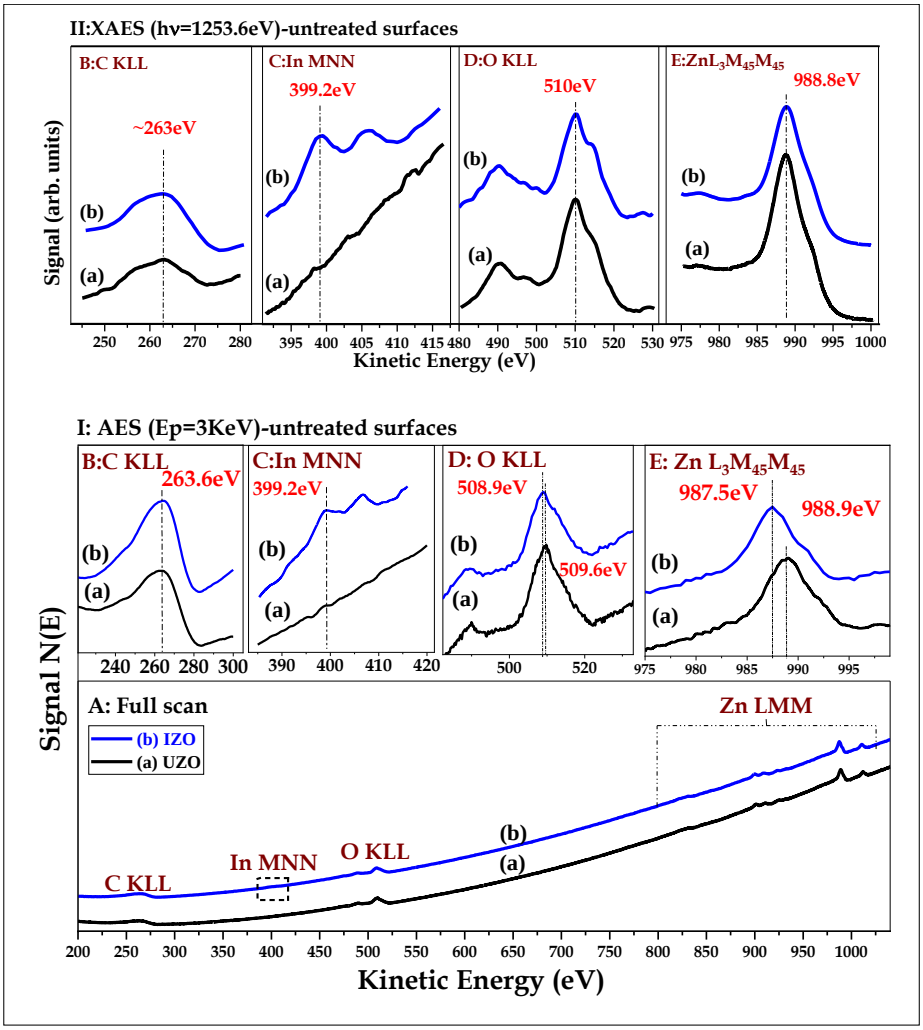

Figure 2: AES (I) and X-AES (II) spectra of as-prepared UZO (a) and IZO (b) thin films (at the initial state). A: AES spectra (Full scan), B, C, D and E: Well resolved Auger transitions of C KLL, In MNN O KLL and Zn $L_3M_{45}M_{45}$.I: AES (Auger Electrons induced by the electron excitation); X-AES (Auger Electrons induced by the X Ray excitation)

3.2.XPS and AES Results of treated surfaces:

The main purpose of Ar^+ etching and UHV annealing is to remove the contamination layer and disposal of some species like hydroxyl and water from bulk. The process of UHV treatment has been achieved as described previously in section 2.2 in order to improve the

chemical, optical and morphological properties of ZnO thin films **[42]**. In **figure 3**, we exhibit the XPS spectra of treated UZO and IZO surfaces. The full scan XPS spectra show a significant improvement of signals related to zinc and oxygen in comparison with those shown at the initial state in **figure 1**. As shown on the tables in **figure 3-A,** both samples are almost of same at% proportion of oxygen (~57%). But, the at% of zinc are 37.14% and 34.68% for UZO and IZO respectively. There is less of zinc in IZO in comparison with UZO because of the incorporation of indium in the ZnO matrix. The Ar ion etching treatment and high temperature annealing led to the desorption of zinc atoms from ZnO surface and the segregation of In impurities with substantial change in the surface structure **[46]**. The kinetic energies related to the main Auger transition In $M_5N_{45}N_{45}$ of indium (at the metal state: In-In and oxidized state: In_2O_3) are 402.6eV **[47]** and 398.6eV **[48]** respectively. We note that the kinetic energy of Auger electrons of the transition In $M_5N_{45}N_{45}$ on **figure 4** is at intermediate value 399.2eV corresponding to the chemical bond Zn-O-In in agreement with the previous XPS results. The UHV physical treatment allows creating a new atomic arrangement so that the indium atoms replace a part of zinc atoms to constitute a stable chemical structure Zn-O-In with oxygen for which the $In/(In+Zn)$ ratio is of 8.5%. It is also worth to indicate that the UHV physical treatment allows to eliminate the contamination layer from the IZO surface (the peaks related to carbon C KLL and C 1s are significantly reduced). Besides, the signal related to indium In MNN increases in intensity as shown in **figure 4**. The intensity of Auger transition In MNN is higher in X-AES (Auger signal obtained by X Ray excitation) than AES one (Auger signal obtained by electron excitation). This result is justified by the excited depth by X Ray (X-AES) more important than the one excited by the electrons (AES). Furthermore, the shape of In MNN transition of band structure type allows us to show the homogeneity of the physical and chemical structure in bulk and surface based the bonds Zn-O-In type as previously described. Furthermore, the shifts of Zn 2p3/2 and O1s peaks of 0.55 and 0.35eV respectively are important in comparison with those mentioned in the initial state (discussed in section 3.1). These shifts are due to the arrangement of indium atoms in the ZnO matrix advantaged by the UHV physical treatment.

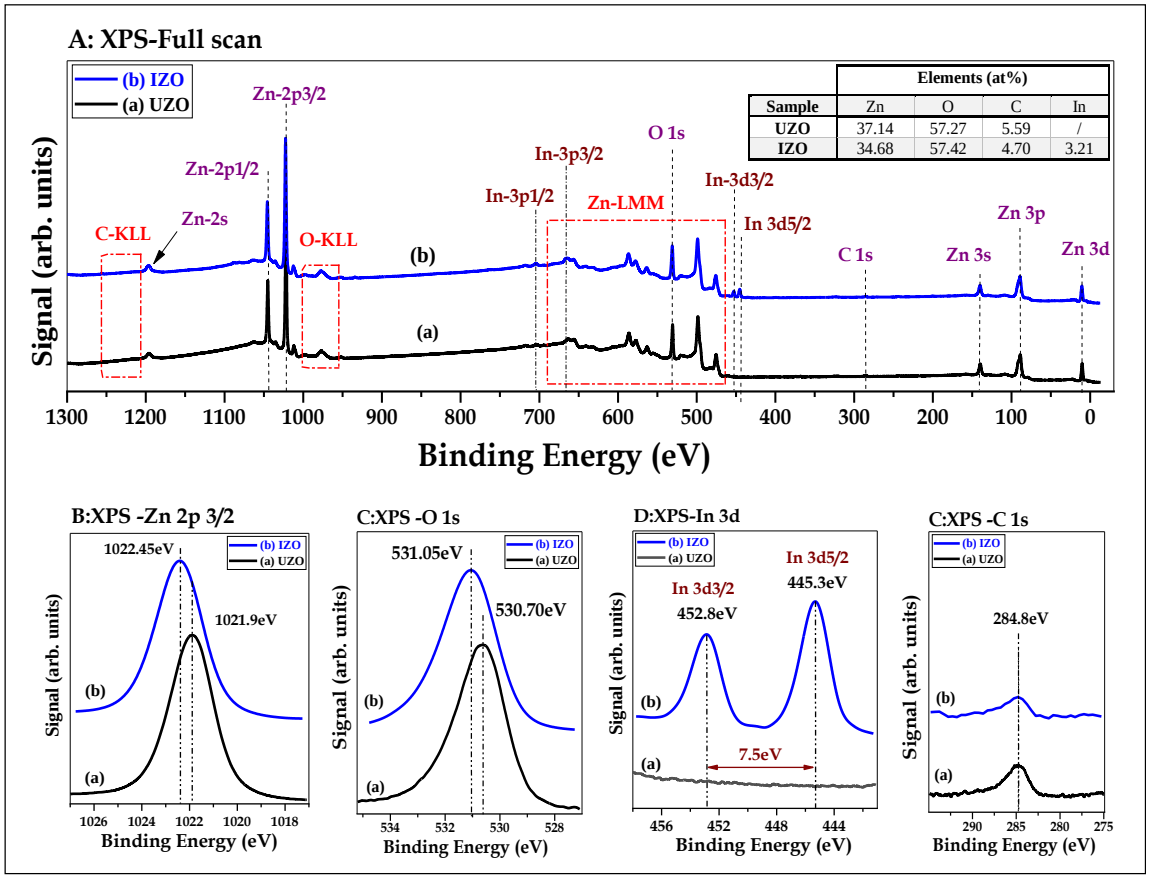

Figure 3: XPS spectra of treated UZO (a) and IZO (b) thin films. A: full scan; B, C, D and E: the well-resolved photoemission spectra of Zn2p3/2; O-1s, In 3d and C 1s respectively.

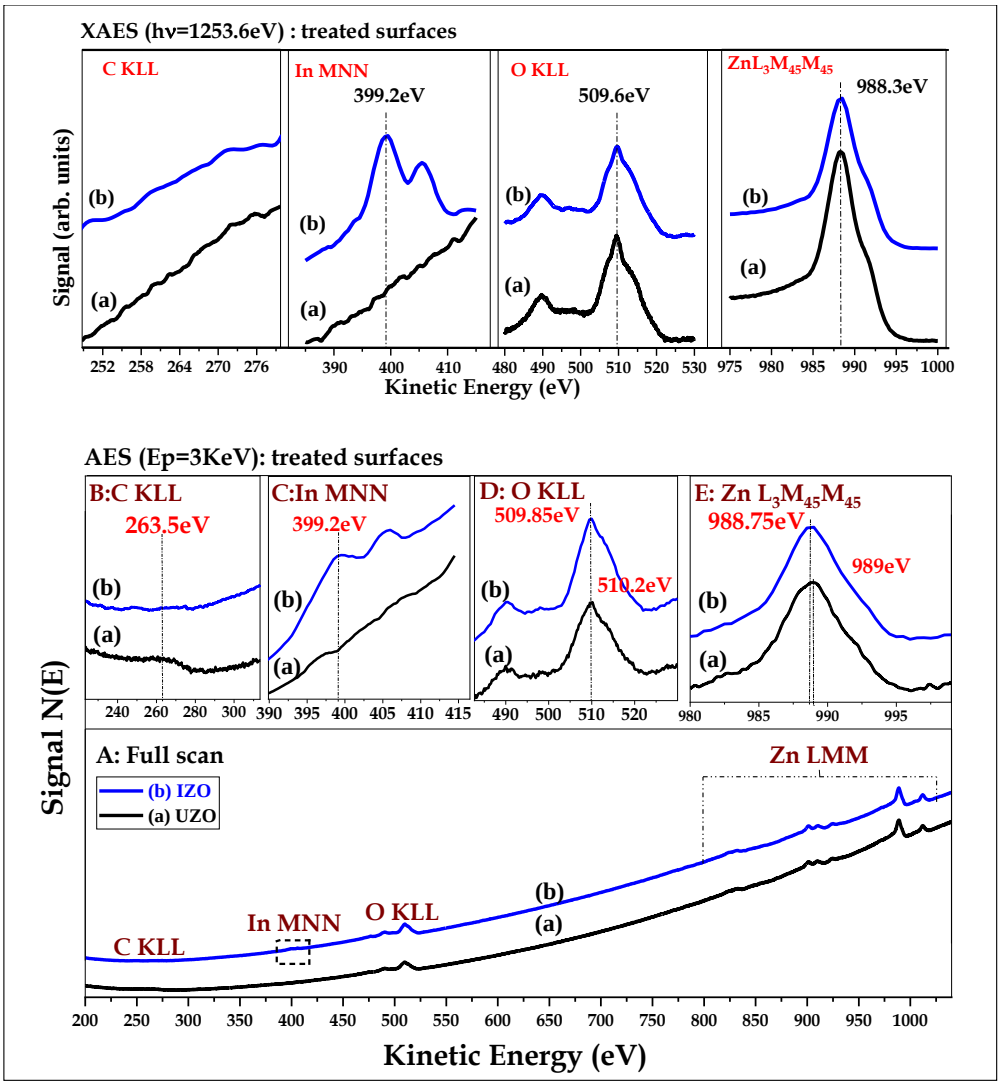

Figure 4: AES(I) and X-AES(II) spectra of UZO and IZO treated surfaces. A: AES spectra (Full scan), B, C, D and E: Well resolved Auger transitions of C KLL, In MNN, O KLL and Zn $L_3M_{45}M_{45}$.

3.3. PL results

The room temperature PL spectra of UZO and IZO thin films were recorded before and after UHV treatment as shown in **figure 5**. Both samples offer a strong UV luminescence at 3.27eV (379nm) ascribed to near band-edge emission (NBE) due to the recombination of free excitons **[48,49]**. The band gap is of 3.33eV by taking into account the displacement due to energy exciton of 60meV from the band edge **[50]**, as shown in **figure 6**. We calculate the FWHM (Full Width at Half Maximum) of the NBE peak of UZO and IZO compounds. We deduce that the NBE peak is very sensitive to the bandgap fluctuation induced by extrinsic defects. The little increase of FWHM from 17nm (for UZO-a1) to 17.5nm (for UZO-a2) indicates that the UHV treatment is efficient to improve the state of the UZO surface. For In

doping effect, the FWHM increases from 26.2nm for the as-prepared IZO thin film (at the initial state) to reach the value 30.3nm after the UHV physical treatment. These results show that the UHV treatment induces the incorporation of In atoms into the ZnO matrix as confirmed previously by the XPS and AES results**.** Since the atomic radii of the In^{3+} ion (0.080 nm) is bigger than the Zn^{2+} one (0.074 nm), the incorporation of indium into the ZnO matrix is susceptible to cause structural defects **[51]**. Thus, we see the asymmetric UV peak of IZO with a slight shoulder corresponding to IZO-b2 spectrum (shown in figure 5-II: Near UV-emission after treatment) of higher FWHM. As reported in the literature, the suggested emissions are related to electron transitions from the Zn_i and extended Zn_i states to valence band maximum [$Zn_i \rightarrow VB$ and extended $Zn_i \rightarrow VB$] at 3.11 eV (400 nm) and around 2.7-2.8 eV (460-440 nm) respectively. Besides, other suggested emissions corresponding to $CB \rightarrow V_{Zn}$ and $Zn_i \rightarrow V_{Zn}$ transitions at 3.03eV (~410nm) and 2.81 eV (441nm) respectively are shown on the ZnO band diagram **[50, 52-55]**, (see **figure 6**). In addition, on the basis of Gaussian fitting of UV peak, numerous literatures reported that the integrated peak area ratio of defect emission to NBE emission (I_{Zni}/I_{NBE}) could be used to describe semi-quantitatively the defect density **[56,57]**. Zhang et al. **[52]** reported that the enhanced ratios of I_{Zni}/I_{NBE} for IZO thin films reveal that In-doping induces high level of Zn_i-related to shallow donor defects. On the basis of these results, we suggest that the incorporation of indium into the clean ZnO matrix increases the level of Zn_i and V_{Zn} defects inducing a broadening in the NBE emission.

The visible emission attributed to defects is generated during the deposition process. The first layers over the surface of ZnO thin films elaborated by chemical synthesis consist of surface defects as dangling bonds, precipitates/segregations/organic residues, surface OH^- ions and other intrinsic defects **[58].** We have identified in a recent study the contamination species (OH, H_2O, and CO_x) and investigated its effect on the chemical properties of ZnO using AR-XPS (Angle Resolved-XPS) **[42]**. Also, as reported, the presence of $Zn(OH)_2$ and hydroxyl groups at the surface, especially for thin films prepared by solution methods affect the luminescence emission phenomenon from ZnO **[59-64]**. As shown in **figure 5**, the signal related to defects around 540nm reduces significantly for UZO and disappears completely for IZO after the UHV treatment. These structural defects are due to interstitial oxygen O_i or contamination species **[41,65-69]**. They are more important for UZO through its luminescence signal around 540nm which is intense and less resolved. As shown previously in XPS and AES results, the UHV treatment is efficient to remove the contamination layer and improve

the chemical state through the atomic arrangement on the surface **[42]**. Besides, due to more Zn_i contribution in IZO, the emission around 620 nm (~2eV) shown by spectrum IZO-b1 may be attributed to the $Zn_i \rightarrow O_i$ transition.

For both samples, there is also a Near IR luminescence displaying two peaks at the initial state (as prepared sample) located at 1.65 and 1.6eV (750 and 775nm respectively) as shown in **figure 5-III**. Stavale et al. **[70]** suggested that the V_O defect locates in the middle of the bandgap, justified by the emission at 730 nm (1.7 eV) due to the electron recombination from the Vo defect level to the valance band maximum $V_O \rightarrow VB$. Furthermore, Xu et al. suggested that the energy emission (1.7eV) generated by the $CB \rightarrow V_O$ transition **[62]**. Thus, in agreement with these results, we suggest that the first peak at 1.65eV corresponds to $V_O \rightarrow VB$ and/or $CB \rightarrow V_O$ transitions. We also note that the middle of the band gap is at 1.65eV as shown on the band diagram in figure 6. The second peak at 1.6 eV does appear before the UHV treatment for both samples. Based on the band diagram shown on figure 6, the H_i impurity level (hydrogen) is suggested to be below the CB at 0.05eV **[71,72]**. The UZO and IZO surfaces are contaminated at the initial state (before the UHV treatment), the hydrogen impurity might be among chemical species of the contamination layer. So, a luminescence emission might be generated through the $H_i \rightarrow V_O$ transition. The luminescence peak related to that transition reduces significantly for both samples after the UHV treatment.

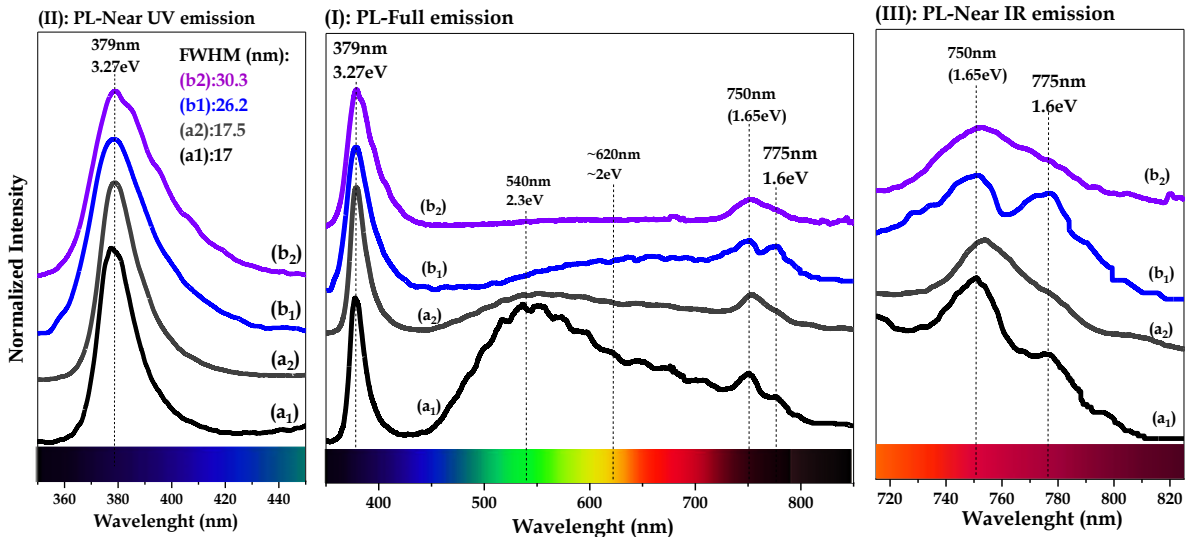

figure 5: (I): Room temperature photoluminescence spectra of UZO (a) and IZO (b) thin films recorded before (a_1 and b_1) and after (a_2 and b_2) the UHV treatment. (II) and (III): the amplified of near UV and near IR emissions respectively.

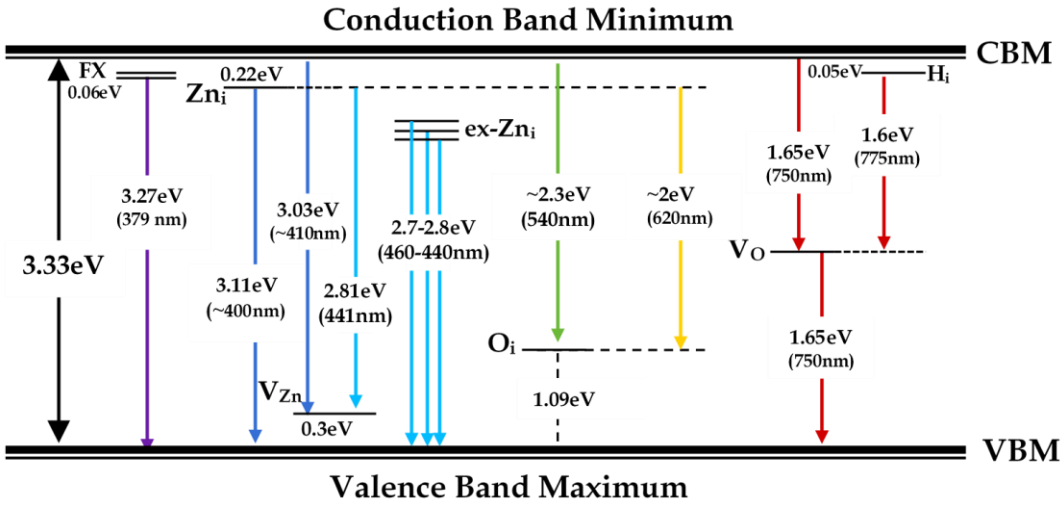

Figure 6: ZnO band diagram with the approximate positions of defect levels and luminescence mechanisms. The band gap is estimated to be 3.33 eV. The luminescence mechanisms are proposed on the basis of the ZnO defect levels suggested by different authors: FX (free exciton) [50]; Zn_i (zinc interstitial), ex-Zn_i (extended Zn_i) and V_{Zn} (zinc vacancies)[50, 52-55, 67, 71,72], O_i (oxygen interstitial) [50,53,69], H_i (hydrogen interstitial) [71, 72], V_O (oxygen vacancies) [62,70].

3.1.UPS results:

UPS technique is complementary to AES and XPS as it gives the electronic structure of upper layers of ZnO film. The electronic properties of the interfaces between ZnO and other component in devices are strongly depending on the work function and electronic structure near the valence band of ZnO surface **[73].** In this regard**,** we use UPS to analyze the surface electronic structure and determine the Fermi level position with respect to the valence band maximum $\left(E_F - E_{VBM}\right)$, the work function $\left(WF = E_{vac} - E_F\right)$ and the ionization potential $\left(I_P = E_{vac} - E_{VBM}\right)$ of UZO and IZO thin films before and after the UHV treatment. The cut-off's maximum intensity allows the determination of the surface work function of studied samples according to $WF = h\nu - E_{cut-off}$ where $h\nu$ is the excitation energy (here 21.2eV) and $E_{cut-off}$ the interception point of the background line and the linear extrapolation of high energy cut-off. The ionization energy corresponds to $I_P = WF + \left(E_F - E_{VBM}\right)$ with $E_F - E_{VBM}$ the energy difference between the valence band maximum and the Fermi level position **[74]**. The work function of material is depending on the Fermi level position $\left(E_F - E_{VBM}\right)$ and the ionization potential I_P **[75]**. The cut-off and valence band maximum regions display the

change of WF and $E_F - E_{VBM}$ of samples as indicated in **figure7-A(I, III) and 7-B (I, III).** We summarize the values of WF, $E_F - E_{VBM}$ and I_P in **table 1.**

For treated surfaces in **figure7-B**, the three main features of UPS spectra can be assigned to the electronic structures corresponding to Zn 3d (10.8 eV), Zn 4s–O 2p mixing contribution (~6 and ~7.5 eV) and O 2p (4.6 eV) related states **[76,77]**. Gutmann et al. **[77]** reported that the reintroduction of a contamination layer reduced the emissions from the ZnO surface, and introduced additional emissions in the range between 5 and 8 eV, related to adsorbed water and hydrocarbons. The UPS spectra of UZO and IZO thin films at the initial state (as prepared sample) are shown in **figure 7A**. These spectra are of similar shape with first peak at 11.2eV and another broad peak in the energy range (4.5 -8.5eV) attributed to (Zn 3d) and (C2s/Zn4s-O2p) respectively. For treated UZO and IZO thin films (see figure 7B), there are three resolved features of UPS spectra assigned to the electronic structure Zn3d at 10.8eV, hybridization of (Zn 4s and O2p) in the energy range (6 -7.5eV) and O2p at 4.6eV in agreement with reported results **[76]**. The shapes of these UPS spectra are similar but we notice that after physical treatment, the intensity of the electronic structure signals for IZO is better than that of UZO. Furthermore, we discuss the UPS results based on physical parameters of great importance which are the work function, the Fermi level position, and the ionization potential defined previously and well highlighted in a recent study **[78].** First of all, it should be noted that the calculated WF is affected by the contamination layer **[79]**, the thermal annealing temperatures **[80],** the bias voltage **[81]** and takes into account the concentration and type of doping **[81]**. The convenient value of the WF corresponds to clean state of the surface **[82].** Klein et al **[83]** showed the importance of Fermi level and work function for the photovoltaic based on transparent conducting oxides. The effect of treatment on both samples induces the variation of work function WF so that (UZO: 4.4eV to 5eV and IZO: 4.5eV to 5.2eV). So, the physical treatment allows the enhancement of the work function. On the other hand, the initial incorporation of indium into the ZnO matrix (untreated surfaces) induces a shift of 0.06eV in the WF while this shift becomes more important (0.2eV) after treatment. Therefore, as shown in the XPS and PL results, the UHV treatment, stimulates the incorporation and oxidation of more indium in the ZnO matrix. The increase of the work function allows the decrease of Femi level position $\left(2.95 \rightarrow 2.86eV\right)$ for IZO and $\left(3.26 \rightarrow 3eV\right)$ for UZO. This result is in agreement with the reported one by Klein et al. **[75]**. They considered that the formation of zinc vacancies, as acceptor states, leading to decrease

the Fermi level position for Al-ZnO. We previously showed the incorporation of indium (justified by the XPS analysis) causes the increase of the zinc vacancies level (justified by the PL analysis). Also, the physical treatment increases the ionization potential I_p (7.66eV to 8.00eV for UZO) and (7.45eV to 8.06eV for IZO) which indicates that there is a development of a surface dipole. Here, modification of the surface dipole is attributed to the new atomic arrangement of new upper layers emerging after Ar^+ cleaning (removal of contamination layer) and annealing at high temperature (removal of adsorbed contaminants) **[75, 84]**.

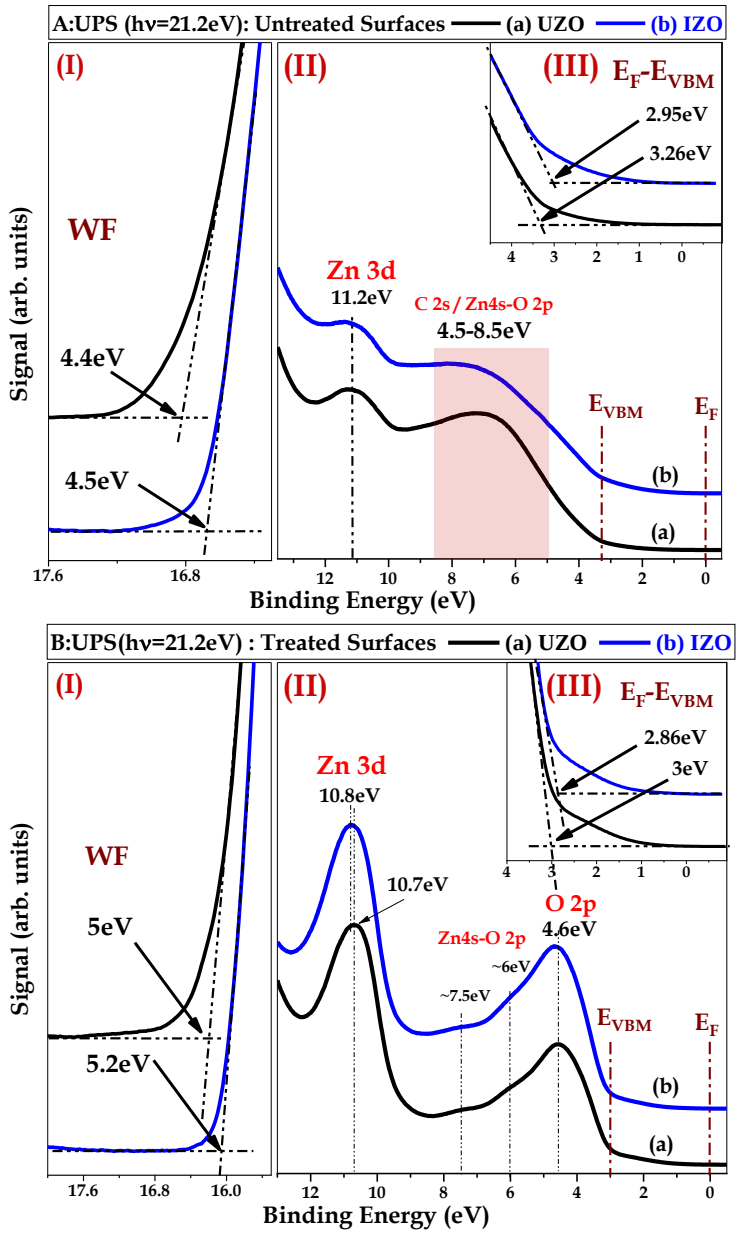

Figure 7: UPS spectra of (a) UZO and (b) IZO recorded before (A) and after (B) treatment and showing (I) secondary electron cut-off (for determine WF), (II) electronic structure of valence band region, and (III) close-up of valence band maximum and bandgap region (for determine E_F-E_{VBM}).

		$WF(eV)$	$E_F - E_{VBM}(eV)$	$I_P = WF + (E_F - E_{VBM})(eV)$
UZO	**Untreated**	4.40	3.26	7.66
	Treated	5.00	3.00	8.00
IZO	**Untreated**	4.50	2.95	7.45
	Treated	5.2	2.86	8.06

Table 1: The work function (WF) and Fermi level position ($E_F - E_{VBM}$) of untreated and treated (UZO and IZO) surfaces.

4. Conclusion

In this study, the undoped and In(6%)-doped zinc oxide (UZO and IZO) thin films deposited on Si substrate are treated in UHV (Ultra-high Vacuum) under the same conditions by Ar^+ ion etching followed by thermal annealing at 650°C. The powerful complementary analysis techniques XPS (X-rays Photoelectron Spectroscopy), AES (Auger Electron Spectroscopy) and UPS (UV Photoelectron Spectroscopy) associated with PL (Photoluminescence) are of great sensitivities to characterize the chemical composition, optical properties and electronic structure of both samples. The AES and XPS results display, through the well-resolved spectra, the effectiveness of the spray technique in the preparation of homogeneous undoped and In-doped ZnO (UZO and IZO) thin films. The UHV physical treatment stimulates the indium incorporation and oxidation into clean ZnO matrix with good structural homogeneity in surface and bulk involving chemical bonds of type Zn-O-In. The photoluminescence constitutes a good means to determine the nature of structural defects. Furthermore, we use the complementary UPS technique for showing the electronic structure, work function and Fermi level position of both samples.

5. References

[1]. Z. C. Feng, Handbook of Zinc Oxide and Related Materials: Volume One, Materials (Electronic Materials and Devices), Taylor & Francis Group, CRC Press 2013.

[2]. A. Mang, K. Reimann, Band gaps, crystal-field splitting, spin-orbit coupling, and exciton binding energies in ZnO under hydrostatic pressure, Solid state communications, 94.4 (1995): 251-254. https://doi.org/10.1016/0038-1098(95)00054-2.

[3]. A. Janotti, C. G. Van de Walle, Fundamentals of zinc oxide as a semiconductor. Reports on progress in physics, 72.12 (2009): 126501. https://doi.org/10.1088/0034-4885/72/12/126501.

[4]. P. Rong, S. Ren, Q. Yu, Fabrications and Applications of ZnO Nanomaterials in Flexible Functional Devices-A Review, Critical Reviews in Analytical Chemistry. 49.4 (2019) 336-349. https://doi.org/10.1080/10408347.2018.1531691.

[5]. Hu G, Li SQ, Gong H, Zhao Y, Zhang J, Wijesinghe TLSL, et al., White light from an indium zinc oxide/ porous silicon light-emitting diode. J. Phys. Chem. C. 2009; 113: 751–754. https://doi.org/10.1021/jp808432f.

[6]. Wienke J, van der Zanden B, Tijssen M, Zeman M. Performance of spray-deposited ZnO:In layers as front electrodes in thin-film silicon solar cells. Sol. Energy Mater. Sol. Cells. 2008; 92: 884–890. https://doi.org/10.1016/j.solmat.2008.01.023.

[7]. K. Matsubara, P. Fons, K. Iwata, A. Yamada, K, et al., ZnO transparent conducting films deposited by pulsed laser deposition for solar cell applications. Thin Solid Films. 2003; 431–432: 369–372. https://doi.org/10.1016/S0040-6090(03)00243-8.

[8]. M. Kumar, L. Wen, B.B. Sahu, J.G. Han, Simultaneous enhancement of carrier mobility and concentration via tailoring of Al-chemical states in Al-ZnO thin films. Appl. Phys. Lett. 2015; 106: 241903. https://doi.org/10.1063/1.4922732.

[9]. S. Dutta, S. Chattopadhyay, A. Sarkar, M. Chakrabarti, D. Sanyal, D. Jana, Role of defects in tailoring structural, electrical and optical properties of ZnO. Progress in Materials Science, 54.1 (2009): 89-136. https://doi.org/10.1016/j.pmatsci.2008.07.002.

[10]. J. A. Sans, J. F. Sánchez-Royo, A. Segura, G. Tobias, E. Canadell, Chemical effects on the optical band-gap of heavily doped ZnO: M_{III} (M= Al, Ga, In): an investigation by means of photoelectron spectroscopy, optical measurements under pressure, and band structure calculations. Physical Review B, B 79.19 (2009): 195105. https://doi.org/10.1103/PhysRevB.79.195105.

[11]. C. S. Hong, H. H. Park, J. Moon, H. H. Park, Effect of metal (Al, Ga, and In)-dopants and/or Ag-nanoparticles on the optical and electrical properties of ZnO thin films, Thin Solid Films 515.3 (2006): 957-960. https://doi.org/10.1016/j.tsf.2006.07.055.

[12]. K. U. Sim, S. W. Shin, A. V. Moholkar, J. H. Yun, J. H. Moon, J. H. Kim, (2010). Effects of dopant (Al, Ga, and In) on the characteristics of ZnO thin films prepared by RF magnetron sputtering system. Current Applied Physics, 10.3 (2010): S463-S467. https://doi.org/10.1016/j.cap.2010.02.028.

[13]. M. Ahmad, J. Zhao, J. Iqbal, W. Miao, L. Xie, R. Mo, J. Zhu, Conductivity enhancement by slight indium doping in ZnO nanowires for optoelectronic applications, Journal of Physics D: Applied Physics, 42.16 (2009): 165406. https://doi.org/10.1088/0022-3727/42/16/165406.

[14]. Z. Zhu, B. Li, J. Wen, Z. Chen, Z. Chen, et al., Indium-doped ZnO horizontal nanorods for high on-current field effect transistors, RSC advances, 7.87 (2017): 54928-54933. https://doi.org/10.1039/C7RA09105B.

[15]. L. S. Kuan & G. G. K. Liang, Structural and electrical properties of single crystal indium doped ZnO films synthesized by low temperature solution method, Journal of crystal growth, 312.3 (2010): 437-442. https://doi.org/10.1016/j.jcrysgro.2009.10.062.

[16]. A. Singh, S. Chaudhary, D. K Pandya, High conductivity indium doped ZnO films by metal target reactive co-sputtering , Acta Materialia 111 (2016): 1-9. https://doi.org/10.1016/j.actamat.2016.03.012.

[17]. M. Girtan, M. Kompitsas, R. Mallet, I. Fasaki, On physical properties of undoped and Al and In doped zinc oxide films deposited on PET substrates by reactive pulsed laser deposition, The European Physical Journal-Applied Physics, 51.3 (2010). https://doi.org/10.1051/epjap/2010112.

[18]. M. Girtan, M. Socol, B. Pattier, M. Sylla, A. Stanculescu, On the structural, morphological, optical and electrical properties of sol–gel deposited ZnO: In films, Thin Solid Films, 519.2 (2010): 573-577. https://doi.org/10.1016/j.tsf.2010.07.006.

[19]. R. Bel-Hadj-Tahar & A. B. Mohamed, Sol-gel processed indium-doped zinc oxide thin films and their electrical and optical properties, New Journal of Glass and Ceramics, 4.04 (2014): 55. http://dx.doi.org/10.4236/njgc.2014.44008.

[20]. K. Ellmer, R. Mientus, Carrier transport in polycrystalline transparent conductive oxides: A comparative study of zinc oxide and indium oxide. Thin solid films, 516.14 (2008): 4620-4627.https://doi.org/10.1016/j.tsf.2007.05.084.

[21]. Jun Souk, Shinji Morozumi, Fang-Chen Luo, Ion Bita, Flat Panel Display Manufacturing, John Wiley & Sons, 24 sept. 2018.

[22]. David S. Ginley, Hideo Hosono, David C. Paine, Handbook of Transparent Conductors, Springer Science & Business Media, 11 sept. 2010.

[23]. K. Ramamoorthy, K. Kumar, R. Chandramohan, K. Sankaranarayanan, Review on material properties of IZO thin films useful as epi-n-TCOs in opto-electronic (SIS solar cells, polymeric LEDs) devices. Materials Science and Engineering: B 126.1 (2006): 1-15. https://doi.org/10.1016/j.mseb.2005.08.117.

[24]. G. Singh, S.B. Shrivastava, D. Jain, et al., Effect of indium doping on zinc oxide films prepared by chemical spray pyrolysis technique, Bull Mater Sci 33, 581–587 (2010). https://doi.org/10.1007/s12034-010-0089-6.

[25]. S. Mourad, J.E. Ghoul, K. Khirouni, Role of indium doping on structural and electrical properties of ZnO nanoparticles prepared by sol–gel method. J Mater Sci: Mater Electron 31, 6372–6384 (2020). https://doi.org/10.1007/s10854-020-03193-1.

[26]. M. Shaheera, K. G. Girija, M. Kaur, et al., Characterization and device application of indium doped ZnO homojunction prepared by RF magnetron sputtering, Optical Materials 101 (2020): 109723. https://doi.org/10.1016/j.optmat.2020.109723.

[27]. K. Djessas, I. Bouchama, J. L. Gauffier, Z. B. Ayadi, Effects of indium concentration on the properties of In-doped ZnO films: Applications to silicon wafer solar cells, Thin Solid Films 555 (2014): 28-32. https://doi.org/10.1016/j.tsf.2013.08.109.

[28]. E. S. Babu & S. K. Hong, Effect of indium concentration on morphology of ZnO nanostructures grown by using CVD method and their application for H2 gas sensing, Superlattices and Microstructures, 82 (2015): 349-356. https://doi.org/10.1016/j.spmi.2015.02.029.

[29]. A. Hafdallah, F. Yanineb, M. S. Aida, N. Attaf, In doped ZnO thin films. Journal of Alloys and Compounds, 509.26 (2011): 7267-7270. https://doi.org/10.1016/j.jallcom.2011.04.058.

[30]. S. Y. Lim, S. Brahma, C. P. Liu, R. C. Wang, J. L. Huang, Effect of indium concentration on luminescence and electrical properties of indium doped ZnO nanowires. Thin Solid Films 549 (2013): 165-171 https://doi.org/10.1016/j.tsf.2013.09.001.

[31]. M. Caglar, S. Ilican, Y. Caglar, Influence of dopant concentration on the optical properties of ZnO: In films by sol–gel method. Thin Solid Films, https://doi.org/10.1016/j.tsf.2009.03.037.

[32]. R. Yousefi, F. Jamali-Sheini, A. K. Zak, M. R. Mahmoudian, Effect of indium concentration on morphology and optical properties of In-doped ZnO nanostructures. Ceramics International, 38.8 (2012): 6295-6301. https://doi.org/10.1016/j.ceramint.2012.04.085.

[33]. K. J. Chen, F. Y. Hung, S. J. Chang, Z. S. Hu, Microstructures, optical and electrical properties of In-doped ZnO thin films prepared by sol–gel method. Applied Surface Science, 255.12 (2009): 6308-6312.https://doi.org/10.1016/j.apsusc.2009.02.007.

[34]. M. N. Jung, E. S. Lee, T. I. Jeon, et al., Synthesis and investigation on the extrinsic carrier concentration of indium doped ZnO tetrapods, Journal of alloys and compounds, 481.1-2 (2009): 649-653. https://doi.org/10.1016/j.jallcom.2009.03.065.

[35]. C. Zhang, D. Xiong, S. Xu, W. Ouyang, et al., Highly efficient field emission from indium-doped ZnO nanostructure on nanographene/macroporous electric conductive network. Materials Letters 222 (2018): 25-28. https://doi.org/10.1016/j.matlet.2018.03.181.

[36]. C. C. Hsu, C. C. Tsao, Y. H. Chen, X. Z. Zhang, Bipolar resistive switching characteristics of a sol-gel InZnO oxide semiconductor. Physica B: Condensed Matter 561 (2019): 64-69. https://doi.org/10.1016/j.physb.2019.02.048.

[37]. C. Yu, R. Li, T. Li, H. Dong, , W. Jia, B. Xu, Effect of Indium doping on the photoelectric properties of n-ZnO nanorods/p-GaN heterojunction light-emitting diodes. Superlattices and Microstructures, 120 (2018): 298-304. https://doi.org/10.1016/j.spmi.2018.05.060.

[38]. A. Chakraborty, T. Mondal, S. K. Bera, S. K. Sen, R. Ghosh, G. K. Paul, Effects of aluminum and indium incorporation on the structural and optical properties of ZnO thin films synthesized by spray pyrolysis technique. Materials Chemistry and Physics, 112.1 (2008): 162-166. https://doi.org/10.1016/j.matchemphys.2008.05.047.

[39]. S. R. Ardekani, A. S. R. Aghdam, M. Nazari, A. Bayat, E. Yazdani, E. Saievar-Iranizad, A comprehensive review on ultrasonic spray pyrolysis technique: Mechanism, main parameters and applications in condensed matter. Journal of Analytical and Applied Pyrolysis, (2019): 104631. https://doi.org/10.1016/j.jaap.2019.104631.

[40]. C. Falcony, M. A. Aguilar-Frutis, M. García-Hipólito, Spray pyrolysis technique; high-K dielectric films and luminescent materials: a review. Micromachines, 9.8 (2018): 414. https://doi.org/10.3390/mi9080414.

[41]. F. Chang, S. Brahma, J. Huang, et al., Strong correlation between optical properties and mechanism in deficiency of normalized self-assembly ZnO nanorods. Sci Rep 9, 905 (2019). https://doi.org/10.1038/s41598-018-37601-8.

[42]. M. Guezzoul, M. Bouslama, A.Ouerdane, et al., Chemical, morphological and optical properties of undoped and Cu-doped ZnO thin films submitted to UHV treatment. Applied Surface Science (2020): 146302. https://doi.org/10.1016/j.apsusc.2020.146302.

[43]. Y. R. Denny, H. C. Shin, S. Seo, S. K. Oh, et al., Electronic and optical properties of hafnium indium zinc oxide thin film by XPS and REELS. Journal of Electron Spectroscopy and Related Phenomena, 185.1-2 (2012): 18-22. https://doi.org/10.1016/j.elspec.2011.12.004.

[44]. G. C. Park, S. M. Hwang, J. H. Choi, Y. H. Kwon, et al., Effects of In or Ga doping on the growth behavior and optical properties of Zn O nanorods fabricated by hydrothermal process. physica status solidi (a), 210.8 (2013): 1552-1556. https://doi.org/10.1002/pssa.201200907.

[45]. R. Lindsay, C. A. Muryn, E. Michelangeli, G. Thornton, ZnO (0001¯)–O surface structure: hydrogen-free (1× 1) termination. Surface science 565.2-3 (2004): L283-L287. https://doi.org/10.1016/j.susc.2004.07.014.

[46]. J.F. Moulder, W.F. Stickle, P.E. Sobol, K.D. Bomben, Handbook of X-ray Photoelectron Spectroscopy. Physical Electronics Division, Perkin-Elmer Corporation, 1992.

[47]. K. Hamaida, M. Bouslama, M. Ghaffour, F. Besahraoui, et al., Growth of In2O3 on In Metal and on InSb by the Electron Irradiation, Surface Review and Letters 19.06 (2012): 1250066. https://doi.org/10.1142/S0218625X12500667.

[48]. A. Teke, Ü. Özgür, S. Doğan, X. Gu, H. Morkoç, B. Nemeth, et al, Excitonic fine structure and recombination dynamics in single-crystalline ZnO, Physical Review B, 70.19 (2004): 195207. https://doi.org/10.1103/PhysRevB.70.195207.

[49]. Ü. Özgür, Y. I. Alivov, C. Liu, A. Teke, M. A. Reshchikov, S. Doğan, H. Morkoç, A comprehensive review of ZnO materials and devices. Journal of Applied Physics, 98.4 (2005): 11. https://doi.org/10.1063/1.1992666.

[50]. S. Vempati, J. Mitra, P. Dawson, One-step synthesis of ZnO nanosheets: a blue-white fluorophore. Nanoscale research letters, 7.1 (2012): 470. https://doi.org/10.1186/1556-276X-7-470.

[51]. S. Pati, P. Banerji, S. B. Majumder, Properties of indium doped nanocrystalline ZnO thin films and their enhanced gas sensing performance, Rsc Advances 5.75 (2015): 61230-61238. https://doi.org/10.1039/C5RA10919A.

[52]. H. Zhang, W. Li, G. Qin, H. Ruan, Z. Huang, et al., Role of zinc interstitial defects in indium and magnesium codoped ZnO transparent conducting films. Applied Surface Science, 492 (2019): 392-398. https://doi.org/10.1016/j.apsusc.2019.06.245.

[53]. H. Zeng, G. Duan, Y. Li, S. Yang, X. Xu, W. Cai, Blue luminescence of ZnO nanoparticles based on non-equilibrium processes: defect origins and emission controls, Adv. Funct. Mater. 20 (2010) 561–572, https://doi.org/10.1002/adfm.200901884.

[54]. F. Kayaci, S. Vempati, I. Donmez, N. Biyikli, T. Uyar, Role of zinc interstitials and oxygen vacancies of ZnO in photocatalysis: a bottom-up approach to control defect density, Nanoscale 6 (2014) 10224–10234, https://doi.org/10.1039/C4NR01887G.

[55]. Chetan C. Singh, Emila Panda, Zinc interstitial threshold in Al-doped ZnO film: effect on microstructure and optoelectronic properties, J. Appl. Phys. 123 (2018) 165106, https://doi.org/10.1063/1.5021736.

[56]. A. Asok, A.R. Kulkarni, Mayuri N. Gandhi, Defect rich seed mediated growth: a novel synthesis method to enhance defect emission in nanocrystals, J. Mater. Chem. C 2 (2014) 1691–1697, https://doi.org/10.1039/C3TC32107J.

[57]. P. Bappaditya, D. Sarkar, P.K. Giri, Structural, optical, and magnetic properties of Ni doped ZnO nanoparticles: correlation of magnetic moment with defect density, Appl. Surf. Sci. 356 (2015) 804–811, https://doi.org/10.1016/j.apsusc.2015.08.163.

[58]. A. B. Djurišić, Y. H. Leung, Optical properties of ZnO nanostructures. small, 2.8-9 (2006): 944-961. https://doi.org/10.1002/smll.200600134.

[59]. I. Shalish, H. Temkin, V. Narayanamurti, Size-dependent surface luminescence in ZnO nanowires. Physical Review B, 69.24 (2004): 245401. https://doi.org/10.1103/PhysRevB.69.245401.

[60]. A. B. Djurišić, Y. H. Leung, K. H. Tam, Y. F. Hsu, et al., Defect emissions in ZnO nanostructures, Nanotechnology, 18.9 (2007): 095702. https://doi.org/10.1088/0957-4484/18/9/095702.

[61]. K. H. Tam, C. K. Cheung, Y. H. Leung, A. B. Djurišić, C. C. Ling, et al., Defects in ZnO nanorods prepared by a hydrothermal method. The Journal of Physical Chemistry B, (2006): 20865-20871. https://doi.org/10.1021/jp063239w.

[62]. Y. Xu, B. Bo, X. Gao, Z. Qiao, Passivation Effect on ZnO Films by SF6 Plasma Treatment, Crystals 9.5 (2019): 236. https://doi.org/10.3390/cryst9050236.

[63]. M. Wang, L. Jiang, E. J. Kim, S. H. Hahn, Electronic structure and optical properties of $Zn(OH)_2$: LDA+U calculations and intense yellow luminescence, RSC Advances, 5.106 (2015): 87496-87503. https://doi.org/10.1039/C5RA17024A.

[64]. C. Chandrinou, N. Boukos, C. Stogios, , A.Travlos, PL study of oxygen defect formation in ZnO nanorods. Microelectronics journal, 40.2 (2009): 296-298. https://doi.org/10.1016/j.mejo.2008.07.024.

[65]. C. H. Ahn, Y. Y. Kim, D. C. Kim, S. K. Mohanta, H. K. Cho, (2009). A comparative analysis of deep level emission in ZnO layers deposited by various methods. Journal of Applied Physics, 105.1 (2009): 013502. https://doi.org/10.1063/1.3054175.

[66]. Wu, X. L., Siu, G. G., Fu, C. L., & Ong, H. C. (2001). Photoluminescence and cathodoluminescence studies of stoichiometric and oxygen-deficient ZnO films. Applied Physics Letters, 78.16 (2001): 2285-2287. https://doi.org/10.1063/1.1361288.

[67]. B. Cao, W. Cai, H. Zeng, Temperature-dependent shifts of three emission bands for ZnO nanoneedle arrays. Applied physics letters, 88.16 (2006): 161101. https://doi.org/10.1063/1.2195694.

[68]. D. Li, Y. H. Leung, A. B. Djurišić, Z. T. Liu, M. H. Xie, et al., Different origins of visible luminescence in ZnO nanostructures fabricated by the chemical and evaporation methods. Applied Physics Letters, 85.9 (2004): 1601-1603. https://doi.org/10.1063/1.1786375.

[69]. B. Lin, Z. Fu, Y. Jia, Green luminescent center in undoped zinc oxide films deposited on silicon substrates, Applied physics letters, 79.7 (2001): 943-945. https://doi.org/10.1063/1.1394173@apl.2019.APLCLASS2019.issue-1.

[70]. F. Stavale, N. Nilius, H.J. Freund, STM Luminescence Spectroscopy of Intrinsic Defects in ZnO(000$\bar{1}$) Thin Films. The Journal of Physical Chemistry Letters. (2013). 4.22. 3972-3976. https://doi.org/10.1021/jz401823c.

[71]. A. B. Djurišić, X. Chen, Y. H. Leung, A. M. C. Ng, ZnO nanostructures: growth, properties and applications, Journal of Materials Chemistry, 22.14 (2012): 6526-6535. https://doi.org/10.1039/C2JM15548F.

[72]. A. B. Djurišić, A. M. C. Ng, X. Y. Chen, ZnO nanostructures for optoelectronics: material properties and device applications. Progress in quantum electronics, 34.4 (2010): 191-259. https://doi.org/10.1016/j.pquantelec.2010.04.001.

[73]. E. Fortunato, D. Ginley, H. Hosono, D. C. Paine, Transparent conducting oxides for photovoltaics. MRS bulletin, 32(3), 242-247. https://doi.org/10.1557/mrs2007.29.

[74]. M. Krzywiecki, L.Grządziel, A. Sarfraz, et al., Zinc oxide as a defect-dominated material in thin films for photovoltaic applications–experimental determination of defect levels, quantification of composition, and construction of band diagram, Physical Chemistry Chemical Physics 17.15 (2015): 10004-10013. https://doi.org/10.1039/C5CP00112A.

[75]. A. Klein, C. Körber, A. Wachau, et al., Surface potentials of magnetron sputtered transparent conducting oxides, Thin Solid Films, 2009, vol. 518, no 4, p. 1197-1203. https://doi.org/10.1016/j.tsf.2009.05.057.

[76]. S. Noothongkaew, R. Supruangnet, W. Meevasana, H. Nakajima, S. Limpijumnong, P. Songsiriritthigul, (2009). In situ monitoring of ZnO formation by photoemission spectroscopy, Applied surface science, 256(4), 980-983. https://doi.org/10.1016/j.apsusc.2009.05.135.

[77]. S. Gutmann, M. Conrad, M. A. Wolak, M. M. Beerbom, R. Schlaf, Work function measurements on nano-crystalline zinc oxide surfaces, Journal of Applied Physics, 111.12 (2012): 123710. https://doi.org/10.1063/1.4729527.

[78]. A. Kahn, Fermi level, work function and vacuum level, Materials Horizons 3.1 (2016): 7-10. https://doi.org/10.1039/C5MH00160A

[79]. M. Socol, N. Preda, A. Stanculescu, C. Breazu, C. Florica, et al., IZO deposited by PLD on flexible substrate for organic heterostructures. Applied Physics A, 123.5 (2017): 371. https://doi.org/10.1007/s00339-017-0992-4.

[80]. H. Wu, M. Xue, J. Ou, F. Wang, W. Li, Effect of annealing temperature on surface morphology and work function of ZnO nanorod arrays. Journal of alloys and compounds, 565 (2013): 85-89. https://doi.org/10.1016/j.jallcom.2013.02.172.

[81]. C. Huang, M. Wang, Z. Deng, Y. Cao, et al., Low content indium-doped zinc oxide films with tunable work function fabricated through magnetron sputtering. Semiconductor science and technology, 25.4 (2010): 045008. https://doi.org/10.1088/0268-1242/25/4/045008.

[82]. J. Cui, A. Wang, N. L. Edleman, J. Ni, P. Lee, N. R. Armstrong, T. J. Marks, Indium Tin Oxide Alternatives—High Work Function Transparent Conducting Oxides as Anodes for Organic Light-Emitting Diodes. Advanced materials, 13.19 (2001): 1476-1480. https://doi.org/10.1002/1521-4095(200110)13:19<1476::AID-ADMA1476>3.0.CO;2-Y.

[83]. A. Klein, C. Körber, A. Wachau, F. Säuberlich, Y. Gassenbauer, S. P. Harvey, ... & T. O. Mason, (2010). Transparent conducting oxides for photovoltaics: Manipulation of fermi level, work function and energy band alignment. Materials, 3(11), 4892-4914. https://doi.org/10.3390/ma3114892.

[84]. L. L. Kelly, D. A. Racke, P. Schulz, H. Li, P.Winget, et .al, Spectroscopy and control of near-surface defects in conductive thin film ZnO, Journal of Physics: Condensed Matter 28.9 (2016): 094007. https://doi.org/10.1088/0953-8984/28/9/094007.